



Mitochondrial permeability transition drives the expression, identification and validation of necrosis-related genes in prognostic risk models of hepatocellular carcinoma

Jiaxuan Jin^{1,2}, Mengyuan Wang¹, Yinuo Liu¹, Wei Li¹, Xuemei Zhang^{1^}, Zhuoxin Cheng¹

¹Department of Gastroenterology, The First Affiliated Hospital of Jiamusi University, Jiamusi, China; ²Department of Gastroenterology, Jiamusi Central Hospital, Jiamusi, China

Contributions: (I) Conception and design: X Zhang, J Jin; (II) Administrative support: Z Cheng; (III) Provision of study materials or patients: W Li, M Wang, Y Liu; (IV) Collection and assembly of data: J Jin, M Wang, Z Zuo, Y Liu; (V) Data analysis and interpretation: J Jin, F Zhen, W Li; (VI) Manuscript writing: All authors; (VII) Final approval of manuscript: All authors.

Correspondence to: Xuemei Zhang, MD; Zhuoxin Cheng, MD. Department of Gastroenterology, The First Affiliated Hospital of Jiamusi University, 348 Dexiang Street, Jiamusi 154002, China. Email: xuemeizhang@hrbmu.edu.cn; czx6892551@yeah.net.

Background: Hepatocellular carcinoma (HCC) is a prevalent malignant tumor, and the current treatment methods exhibit various limitations. In recent years, the role of mitochondrial permeability transition-driven necrosis-related genes (MPT-DNRGs) in the pathogenesis and progression of severe diseases, particularly tumors, has garnered significant attention. This study aimed to identify new targets and concepts for MPT-DNRG-targeted therapy in HCC.

Methods: In this study, we utilized HCC-related datasets and MPT-DNRGs to identify differentially expressed genes (DEGs) between HCC patients and control groups. By conducting a cross-analysis of the results of DEGs and MPT-DNRGs, we screened candidate genes. Subsequently, univariate Cox regression and least absolute shrinkage and selection operator (LASSO) regression analysis methods were employed to identify prognostic genes, which were used to construct a risk model and calculate individual risk scores for HCC patients. Additionally, we performed univariate and multivariate Cox regression analyses to identify independent prognostic factors and constructed a column chart based on these factors to predict the survival probability of HCC patients. Furthermore, gene set enrichment analysis (GSEA), the immune microenvironment, chemotherapy drugs, and the expression of prognostic genes between the two groups were analyzed. Finally, the expression of these prognostic genes was further confirmed using reverse transcription-quantitative polymerase chain reaction (RT-qPCR) technology.

Results: In this study, we identified 8,515 DEGs between HCC and control samples. By performing intersection analysis between DEGs and MPT-DNRGs, we pinpointed 15 candidate genes. Subsequently, through univariate Cox regression and LASSO regression analysis, we identified six genes (*LMNB2*, *LMNB1*, *BAK1*, *CASP7*, *LMNA*, and *AKT1*) that were significantly associated with overall survival (OS) in patients. Based on the median risk score, we categorized HCC patients into high-risk and low-risk groups. Kaplan-Meier (KM) survival analysis results demonstrated a significant difference in OS between the two groups, which was further validated through additional assessment. Furthermore, we constructed a nomogram to predict the survival probability of HCC patients. Moreover, GSEA revealed a crucial correlation between these genes and HCC, and highlighted a close association between risk scores and regulatory T cells. We also identified four chemotherapy drugs related to HCC. Finally, in both the training and validation cohorts, *LMNB2*, *LMNB1*, and *LMNA* exhibited high expression levels in tumor samples. Further validation using RT-qPCR confirmed that the expression of all prognostic genes was significantly higher in HCC group compared to the control group.

[^] ORCID: 0009-0001-0898-3190.

Conclusions: This study explored six prognostic genes (*LMNB2*, *LMNB1*, *BAK1*, *CASP7*, *LMNA* and *AKT1*) associated with MPT-DNRGs in HCC, which provides a reference for further research on HCC.

Keywords: Hepatocellular carcinoma (HCC); mitochondrial permeability transition-driven necrosis-related genes (MPT-DNRGs); risk model; nomogram; prognosis

Submitted Aug 20, 2024. Accepted for publication Dec 17, 2024. Published online Feb 26, 2025.

doi: 10.21037/tcr-24-1442

View this article at: <https://dx.doi.org/10.21037/tcr-24-1442>

Introduction

Hepatocellular carcinoma (HCC) is the sixth most prevalent cancer globally and ranks third in cancer-related mortality (1,2). Additionally, 85–90% of liver cancer cases are caused by HCC, affecting both the incidence and mortality rates of liver cancer (3,4). Despite advancements in treatment approaches such as radiofrequency ablation, immunotherapy, hepatectomy, and transarterial chemoembolization (TACE) (5,6), the clinical treatment efficacy for HCC remains suboptimal. This is largely due to HCC being frequently diagnosed in advanced stages, resulting in many patients failing to receive optimal treatment (7). Given the complexity, recurrence, high metastasis, and heterogeneity of advanced

cancer stages, HCC has emerged as one of the deadliest malignant tumors, and even following post-surgical resection (8,9), the survival rate remains low. Consequently, enhancing the prognosis of HCC patients is essential, emphasizing the need to identify potential prognostic indicators and develop early diagnostic models.

Recent study (10) have indicated that various apoptosis pathways influence whether apoptosis occurs through the disruption of mitochondrial membranes. This insight has shifted the focus from traditional nuclear-centered regulatory models to mitochondrial-centered regulatory models. A key change in mitochondria during apoptosis is the mitochondrial permeability transition (MPT). Mitochondria contain transmembrane channels, notably the mitochondrial membrane permeability transition pore (MPTP), located in their inner and outer membranes. When damaged or subjected to pathological stimulation, the MPTP opens irreversibly. This irreversible opening initiates a cascade of events that include a sustained decrease in MPT, oxidative phosphorylation uncoupling, alterations in adenosine triphosphatase (ATPase) activity, and a reduction in adenosine triphosphate (ATP) synthesis (9). These changes ultimately lead to cell death due to energy depletion. Additionally, structurally, the influx of large volumes of small molecular weight substances, such as high concentrations of calcium ions into the mitochondrial matrix, causes a significant increase in matrix volume (11). This expansion results in the rupture of the outer mitochondrial membrane. This event is typically triggered by drastic changes in the intracellular microenvironment, such as severe oxidative stress and abnormal elevations in cytoplasmic Ca^{2+} , and relies on the involvement of cyclophilin D (CypD) (11). Although research on MPT in liver cancer is still nascent, its exploration is crucial. MPT plays a significant role in pathological processes such as cardiac reperfusion and malignancies, including laryngeal cancer, by promoting mitochondrial-mediated cell death and inhibiting malignant cell differentiation (12,13).

Highlight box

Key findings

- Bioinformatics methods were employed to identify necrosis-related genes driven by mitochondrial permeability transition (MPT) in hepatocellular carcinoma (HCC) and to construct a prognostic model. Additionally, an extensive analysis was conducted on the relationship between prognostic genes and immune infiltration, the tumor microenvironment, and chemotherapy drugs.

What is known and what is new?

- MPT plays a significant role in pathological processes such as cardiac reperfusion and malignancies, including laryngeal cancer, by promoting mitochondrial-mediated cell death and inhibiting malignant cell differentiation.
- The study explored the prognostic role of necrosis-related genes driven by MPT in HCC, providing valuable insights for ongoing research into this disease.

What is the implication, and what should change now?

- A prognostic model was developed based on necrosis-related genes driven by MPT. This model can more effectively predict the prognosis of patients with HCC and provide potential targets and a solid foundation for the treatment of this disease. Furthermore, analysis of immune infiltration yields important implications for immunotherapy strategies.

In this work, data were integrated from the International Cancer Genome Consortium (ICGC) database and the University of California, Santa Cruz (UCSC) database, using bioinformatics methods to screen for prognostic genes associated with MPT in HCC. An MPT-driven prognostic analysis of necrosis-related genes was conducted, and survival analysis was performed on HCC patients in the training group to clarify the function of these prognostic genes in HCC.

A MPT-driven necrosis-related genes (MPT-DNRGs) messenger RNA (mRNA) prognostic model for HCC was developed, rigorously validated with data from the validation group, and a risk prognostic model comprising six key genes was identified. In-depth studies were conducted on the associations between these prognostic genes and immune infiltration, the tumor microenvironment, and chemotherapy drugs. The expression levels of these prognostic genes were compared between the HCC group and the control group using reverse transcription-quantitative polymerase chain reaction (RT-qPCR). This study offers significant insights and practical guidance for the diagnosis and clinical application of HCC. We present this article in accordance with the TRIPOD reporting checklist (available at <https://tcr.amegroups.com/article/view/10.21037/tcr-24-1442/rc>).

Methods

Data collection

RNA-seq data for HCC were sourced from the University of California Santa Cruz (UCSC) database (<https://xenabrowser.net/datapages/>), 50 normal controls and 374 tumor samples were used for differential analysis; 368 tumor samples with survival information were used to construct the model. Among the 368 tumor samples, 365 had clinical information. Available online: <https://cdn.amegroups.com/static/public/tcr-24-1442-1.xlsx> lists the clinical information of these samples. Data for 232 ICGC-LIRI-JP samples were also obtained from the ICGC database (<https://dcc.icgc.org/>). For validation, dataset GSE76427 from the Gene Expression Omnibus (GEO) database (<https://www.ncbi.nlm.nih.gov/geo/>), comprising 152 tumor and 52 control samples, was utilized. MPT-driven necrosis-related genes (MPT-DNRGs) were identified from the published literature (12).

Differential expression analysis

The DESeq2 software package (version 1.34.0) (13) was utilized to analyze differentially expressed genes (DEGs) between HCC and the control group in the training set. Selection criteria were established as $P_{adj} < 0.05$ and $|\log_2 \text{fold change (FC)}| > 0.5$. To visualize the changes in DEGs, volcano plots and heatmaps were generated using the ggplot2 (version 3.2.1) (14) and pheatmap (version 1.0.12) (15) packages.

Function enrichment analysis

A set of candidate genes was obtained by extracting the intersection of HCC-related DEGs and MPT-DNRGs. Gene Ontology (GO) and Kyoto Encyclopedia of Genes and Genomes (KEGG) enrichment analyses were performed using the clusterProfiler software package ($P_{adj} < 0.05$) (version 2.13) (16).

Construction of risk model

Univariate Cox regression analysis was conducted using the “survival” package (17) (version 3.3-1) to screen for genes correlated with overall survival (OS) of HCC patients. Next, least absolute shrinkage and selection operator (LASSO) regression analysis was utilized to select prognostic genes. The risk score for all patients was calculated using the formula: Risk score = expression of each gene \times coefficient of each gene. Based on the median risk score, all HCC patients were categorized into high-risk and low-risk groups. OS differences between these groups were analyzed using the log-rank test and Kaplan-Meier (KM) survival curves were drawn for evaluation using the Survminer software package (version 0.4.9) (17). Additionally, “survivalROC” (18) (version 1.0.3) was used to calculate false positive and true positive rates, and the results were used to plot receiver operating characteristic (ROC) curves and perform principal component analysis (PCA). Finally, the model was validated in the validation cohort. In the training and validation datasets, expression differences of prognostic genes between the HCC group and the control group were compared using the Wilcoxon test ($P < 0.05$).

Construction of nomogram

Univariate and multivariate Cox regression analyses were

employed, in conjunction with risk scores and clinical features, to screen for independent prognostic factors. Upon identifying these factors, a nomogram was established using the “rms” package (19) (version 6.5-0). Furthermore, the effectiveness of the nomogram was evaluated using ROC curves and calibration curves.

Gene set enrichment analysis (GSEA)

To further elucidate the biological functions and pathways associated with different risk cohorts, GSEA was conducted on DEGs in the various risk groups. The background gene set `c2.cp.kegg.v7.1.symbols.gmt` and `GO c5.all.v7.1.symbols.gmt` was downloaded from Molecular Signatures Database (MSigDB) (<https://www.gsea-msigdb.org/gsea/msigdb>).

Immune-related analysis

The CIBERSORT algorithm (20) (version 2.0.4) was used to quantitatively analyze 22 types of immune cells and the Wilcoxon test was employed to screen for immune cells with significant differences ($P < 0.05$). Subsequently, Spearman correlation analysis was conducted to explore the correlation between these differential immune cells and prognostic genes, and the results were presented in the form of heatmap. The genes related to checkpoints were obtained from the literature (21), and then the expression data of these genes in the training set was extracted. The difference in gene expression between the two groups was analyzed using the Wilcoxon test ($P < 0.05$).

Drug prediction

To explore chemotherapy drugs correlated with HCC, relevant drug information was searched using the Genomics of Drug Sensitivity in Cancer (GDSC) database (<https://www.cancerrxgene.org>). In the training set, the half maximal inhibitory concentration (IC₅₀) values for each drug in HCC samples were calculated, and the difference in IC₅₀ values for each drug was analyzed through the Wilcoxon test to reveal its inhibitory effect on HCC cells.

Expression analysis of prognosis genes

HepG2 and Huh7 cells, provided by the Cell Bank of the Chinese Academy of Medical Sciences, and LO2 cells, obtained from Icellbioscience Company, were cultured

in Dulbecco's Modified Eagle Medium (DMEM) and Roswell Park Memorial Institute-1640 (RPMI-1640) complete medium (Servicebio, Wuhan, China), containing 10% fetal bovine serum, 1% monoclonal antibody, and 1% N-2-Hydroxyethylpiperazine-N-2-ethane sulfonic acid (HEPES) (Gibico, California, USA). Cultivation conditions involved maintaining a constant temperature of 37 °C and 5% CO₂ in a standard incubator. Following the manufacturer's instructions, one mL of TRIzol reagent (ELK Biotechnology, Wuhan, China) was used to extract total RNA from each sample. The RNA concentration was measured using a NanoPhotometer N50 analyzer. Subsequently, cDNA synthesis was performed from the extracted RNA using the EntiLink™ 1st Strand cDNA Synthesis SuperMix, and reverse transcription was carried out using the S1000™ thermal cycler (Bio-Rad, USA). Quantitative PCR (SLAN-96S) was conducted on the QuantStudio 6 Flex System (Life Technologies, Shanghai, China). The thermal cycling conditions were: pre-denaturation at 95 °C for 30 s, denaturation at 95 °C for 10 s, annealing at 58 °C for 30 s, and extension at 72 °C for 30 s, repeated for 40 cycles. The relative expression level of mRNA was calculated using the $2^{-\Delta\Delta CT}$ method.

Ethical statement

The study was conducted in accordance with the Declaration of Helsinki (as revised in 2013).

Statistical analysis

Data were processed and analyzed using R software (version 4.2.2). $P < 0.05$ was considered statistically significant.

Results

A total of 8,515 DEGs were identified and analyzed for enrichment

There were 8,515 HCC-related DEGs identified between HCC and control samples, including 5,851 upregulated genes and 2,664 downregulated genes (Figure 1A,1B). Next, Venn diagram analysis was used to extract the intersection genes between HCC-related DEGs and MPT-DNRGs, resulting in 15 intersecting genes (Figure 1C). GO and KEGG enrichment analyses were conducted on these intersecting genes to explore their biological functions and related pathways. The analysis results indicated that the

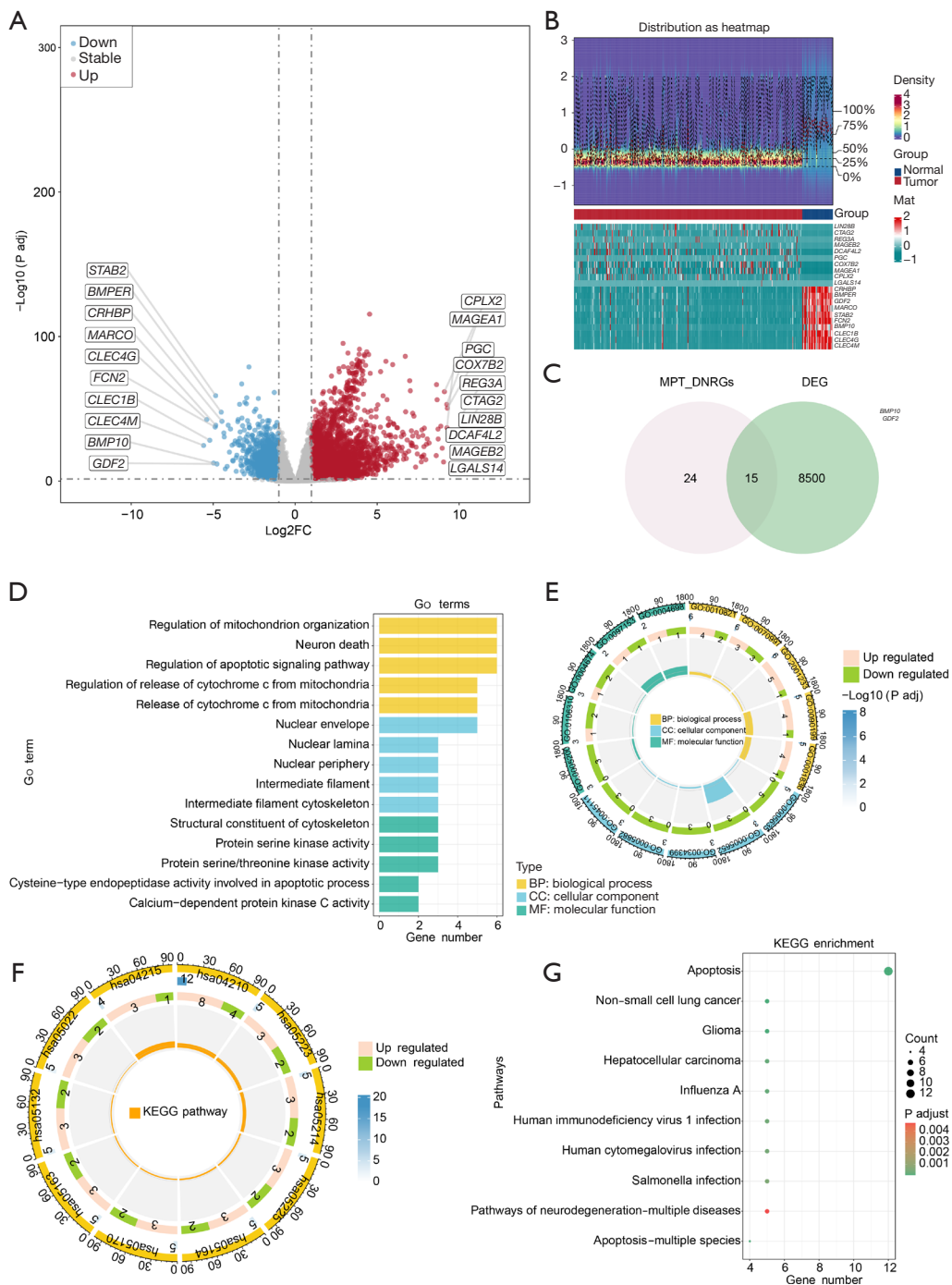


Figure 1 Intersection genes screening and GO, KEGG enrichment analysis. (A,B) were performed to obtain the volcano and heat maps of the DEGs related to LIHC from UCSC database. Top logFC up-down 10 genes were selected for display. (C) Venn diagram of the intersection of LIHC-related DEGs and MPT-DNRGs. (D,E) Go function enrichment analysis of intersection genes. Only TOP5 in descending order of enrichment number is shown for significant (P value <0.05) conditions. (F,G) KEGG pathway enrichment analysis of intersection genes. Only TOP10, in descending order of enrichment number, was shown under significant (P .adj <0.05) conditions. GO, Gene Ontology; KEGG, Kyoto Encyclopedia of Genes and Genomes; DEGs, differentially expressed genes; UCSC, University of California Santa Cruz; FC, fold change; MPT-DNRGs, mitochondrial permeability transition-driven necrosis-related genes; LIHC, liver hepatocellular carcinoma; DEG, differentially expressed gene; BP, biological process; CC, cellular component; MF, molecular function.

intersection genes were associated with mitochondrion organization regulation, nuclear envelope, structural constituent of cytoskeleton, cysteine-type endopeptidase activity, etc. (Figure 1D,1E). Additionally, these intersection genes showed enrichment in KEGG pathways such as apoptosis, glioma, and HCC (Figure 1F,1G).

Selection of OS-related genes in HCC patients

As indicated in Figure 2A, nine genes (*LMNB2*, *LMNB1*, *CASP2*, *BAK1*, *CASP7*, *LMNA*, *PARP1*, *AKT1*, and *BAX*) were found to significantly increase the risk of death. LASSO regression analysis was subsequently performed on these nine genes, resulting in the selection of six risk-related genes (*LMNB2*, *LMNB1*, *BAK1*, *CASP7*, *LMNA*, and *AKT1*) (Figure 2B,2C). Using these six genes, the risk score was calculated using the formula: Risk score = *LMNB2* × 0.188 + *LMNB1* × 0.112 + *BAK1* × 0.089 + *CASP7* × 0.048 + *LMNA* × 0.059 + *AKT1* × 0.024. Based on the median risk score, 184 patients were classified as high-risk, while another 184 were classified as low-risk (Figure 2D-2F). KM survival analysis then demonstrated a significant difference in survival between the two groups (Figure 2G). Time-dependent ROC curve analysis showed good prediction accuracy, with an area under the curve (AUC) of 0.717, 0.638, and 0.613 at 1-, 2-, and 3-year, respectively (Figure 2H). PCA results further confirmed that high-risk and low-risk patients could be distinctly divided into two separate regions (Figure 2I). The model's predictive accuracy was validated using data from the ICGC database (Figure 3A-3C). Validation results confirmed consistency with the training set outcomes, indicating that the OS of all high-risk patients was relatively short (Figure 3D). The AUC of the validation set was 0.752 at one year, 0.674 at two years, and 0.696 at three years (Figure 3E), further verifying the robust predictive performance of the risk model. PCA results were consistent with those of the training set (Figure 3F).

Construction of nomogram

To construct a prognostic model for predicting OS in HCC patients, all clinical features and risk scores were comprehensively considered. Initially, univariate Cox regression analysis revealed significant correlation between OS in HCC and risk score, tumor staging, pathological M stage, and pathological T stage (Figure 4A). A multivariate Cox regression model was then constructed based on these factors, and all were tested against the proportional hazards

(PH) hypothesis (Figure 4B). A nomogram integrating various independent prognostic factors was established (Figure 4C). Using the nomogram, the overall risk score for each patient was calculated, and the training cohort was divided into high-risk and low-risk groups based on the median risk score. The KM survival curve revealed significantly longer OS for low-risk patients compared to high-risk patients (Figure 4D). The AUC of the ROC curve at one year, two years, and three years was 0.73, 0.68, and 0.69, respectively, indicating good predictive capability of the model (Figure 4E). Calibration curve analysis showed that our model's predictions at one, two, and three years closely matched the ideal model (Figure 4F).

GSEA

To elucidate the biological functions and pathways of DEGs, GSEA was performed. This analysis revealed that DEGs were associated with processes such as spindle elongation, xenobiotic catabolic process, and detoxification of copper ion in the GO-biological process (BP) entries (Figure 5A). Additionally, DEGs were linked to cellular structures including DNA replication preinitiation complex, outer kinetochore, chromatoid body, high-density lipoprotein particle, endocytic vesicle lumen, and chylomicron in GO-cellular component (CC) entries (Figure 5B). In the GO-molecular function (MF) entries, significant associations were found between DEGs and molecular activities such as neurotransmitter receptor regulator activity, DNA binding bending, DNA replication origin binding, and alcohol dehydrogenase NADP⁺ activity (Figure 5C). Further KEGG pathway enrichment analysis demonstrated significant enrichment of DEGs in pathways such as DNA replication, primary immunodeficiency, and homologous recombination (Figure 5D).

Analysis of immune infiltration and immune checkpoints

CIBERSORT and Wilcoxon tests were utilized to analyze immune infiltration across different risk groups. The results revealed significant differences in the expression of 11 immune cell types between the high-risk and low-risk groups ($P < 0.05$), including CD8 T cells, resting mast cells, and monocytes (Figure 6A,6B). Spearman correlation analysis was conducted to explore the relationship between differential immune cells and prognostic genes. It was found that the correlation between regulatory T cells and *LMNA* was the most significant ($r = 0.333$, $P < 0.05$) (Figure 6C). Additionally,

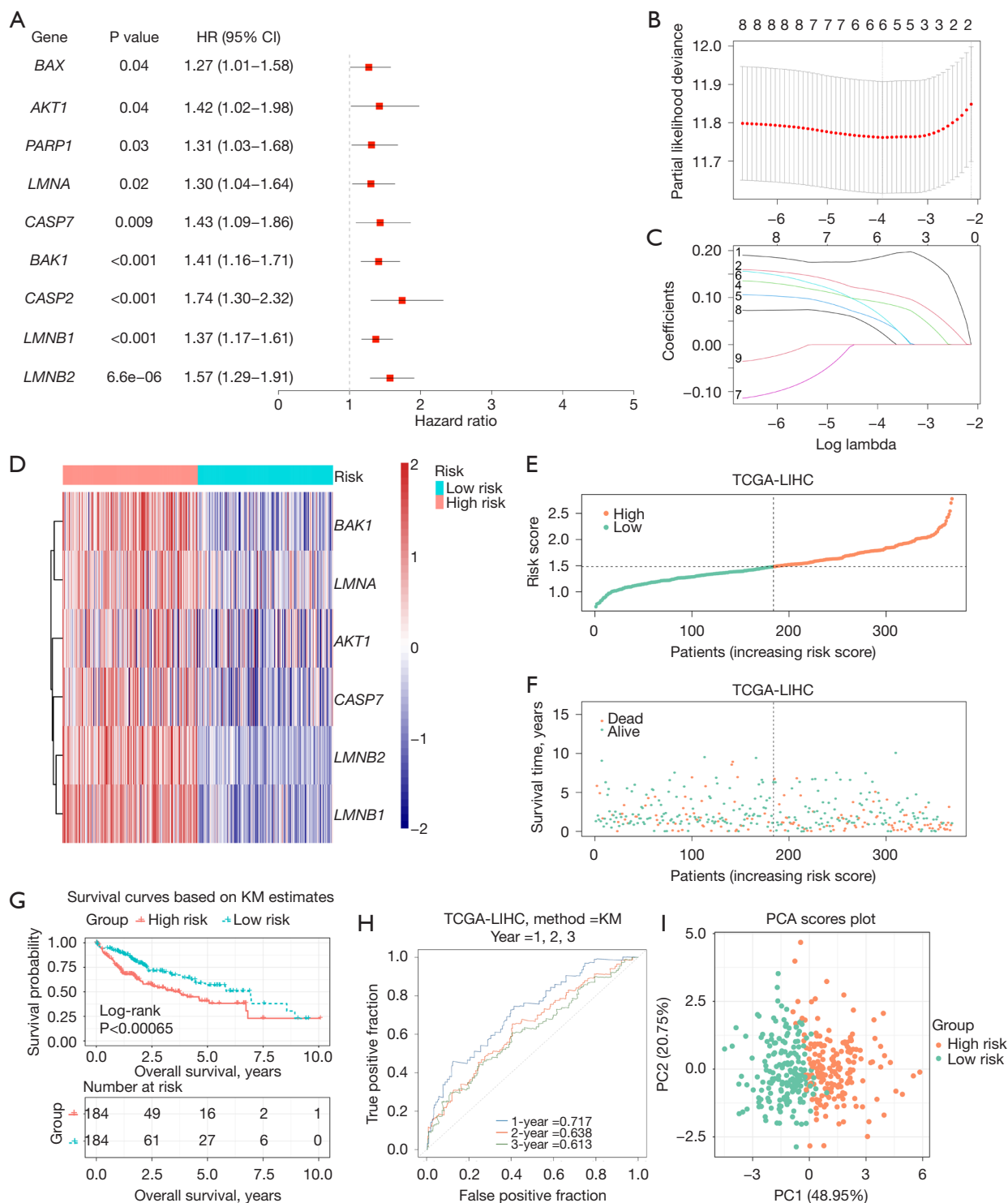


Figure 2 Build a risk model. (A) Univariate Cox analysis of forest plot. (B,C) LASSO regression analysis. (D-F) Heatmap of prognostic genes, training set risk score and survival distribution of patients with LIHC. (G) KM survival analysis for high and low risk groups. (H) ROC curve. (I) PCA analysis. LASSO, least absolute shrinkage and selection operator; KM, Kaplan-Meier; ROC, receiver operating characteristic; PCA, principal component analysis; LIHC, liver hepatocellular carcinoma; HR, hazard ratio; CI, confidence interval; TCGA, The Cancer Genome Atlas.

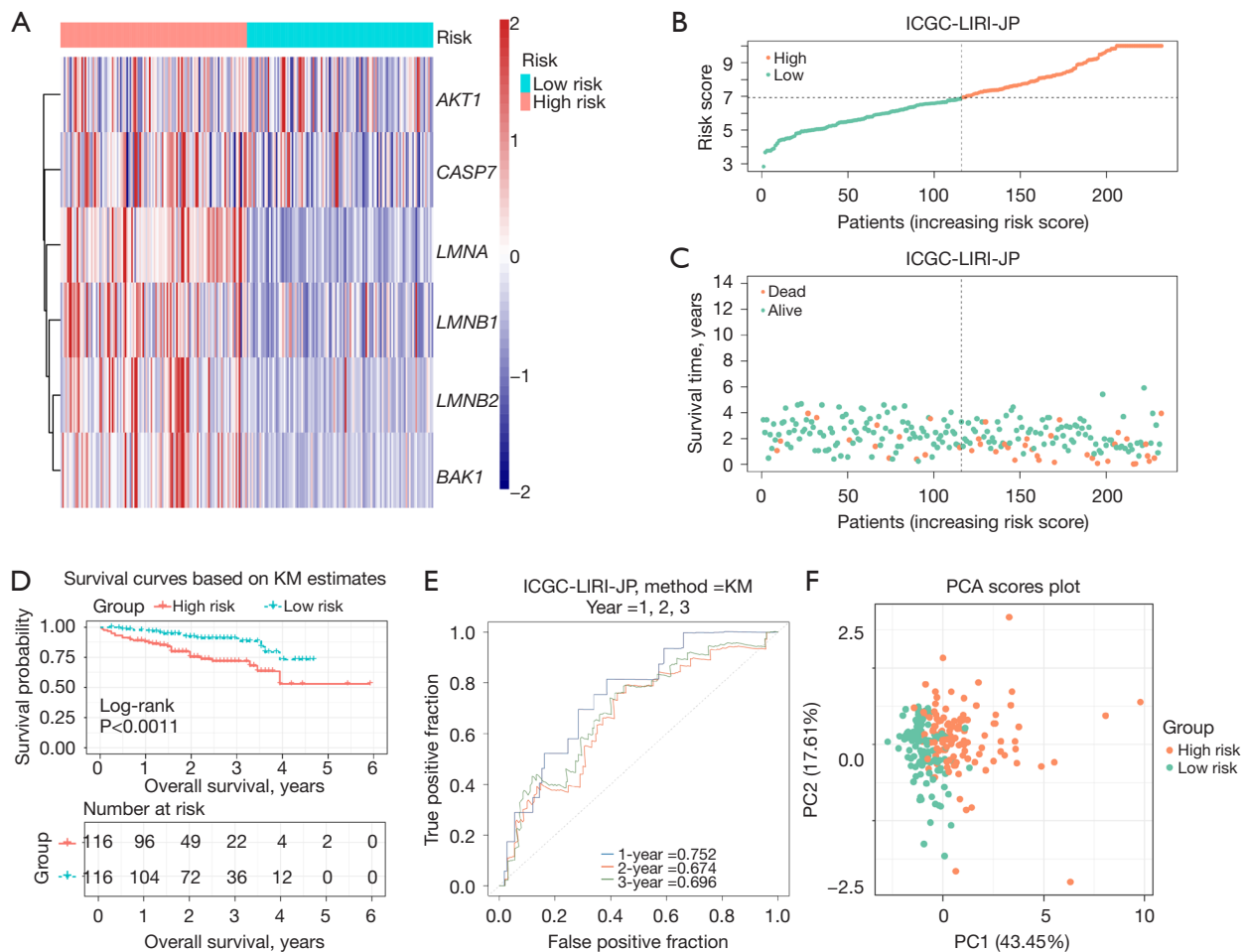


Figure 3 Validation of the risk model. (A-C) Heatmap of prognostic genes, validation set risk score and LIHC patient survival distribution. (D) High-low risk group KM survival analysis. (E) ROC curve. (F) PCA analysis. KM, Kaplan-Meier; ROC, receiver operating characteristic; PCA, principal component analysis; LIHC, liver hepatocellular carcinoma; AUC, area under the curve; ICGC, International Cancer Genome Consortium.

a Wilcoxon test was performed to investigate differences in immune checkpoints between the high-risk and low-risk groups. The results indicated that expressions of immune checkpoints such as *PDCD1*, *ASXL1*, *BCL2*, *CD33*, *CD47*, *PLK1*, *DOT1L*, *FLT3*, *CTLA4*, *MCL1*, and *MDM2* were upregulated in the high-risk group (Figure 6D).

Screen of chemotherapy drugs of HCC

Among the 22 chemotherapy drugs studied, IC50 values for 16 drugs exhibited significant differences, including lapatinib, DMOG, erlotinib, axitinib, bicalutamide, CCT007093, GSK269962A, lenalidomide, SB590885, tipifarnib, bosutinib, embelin, nilotinib, vorinostat,

cisplatin, and QS11 (Figure 7A). Further analysis of positive and negative differences between different risk groups identified four drugs with significant differences: lapatinib, DMOG, cisplatin, and QS11 (Figure 7B-7E). These drugs might be considered potential chemotherapy options for HCC.

Expression of prognostic genes

The expression levels of *LMNB2*, *LMNB1*, and *LMNA* were significantly upregulated in HCC in both the training and validation cohorts (Figure 8A, 8B). Expression levels of these prognostic genes were further assessed in HCC cell lines using RT-qPCR, revealing

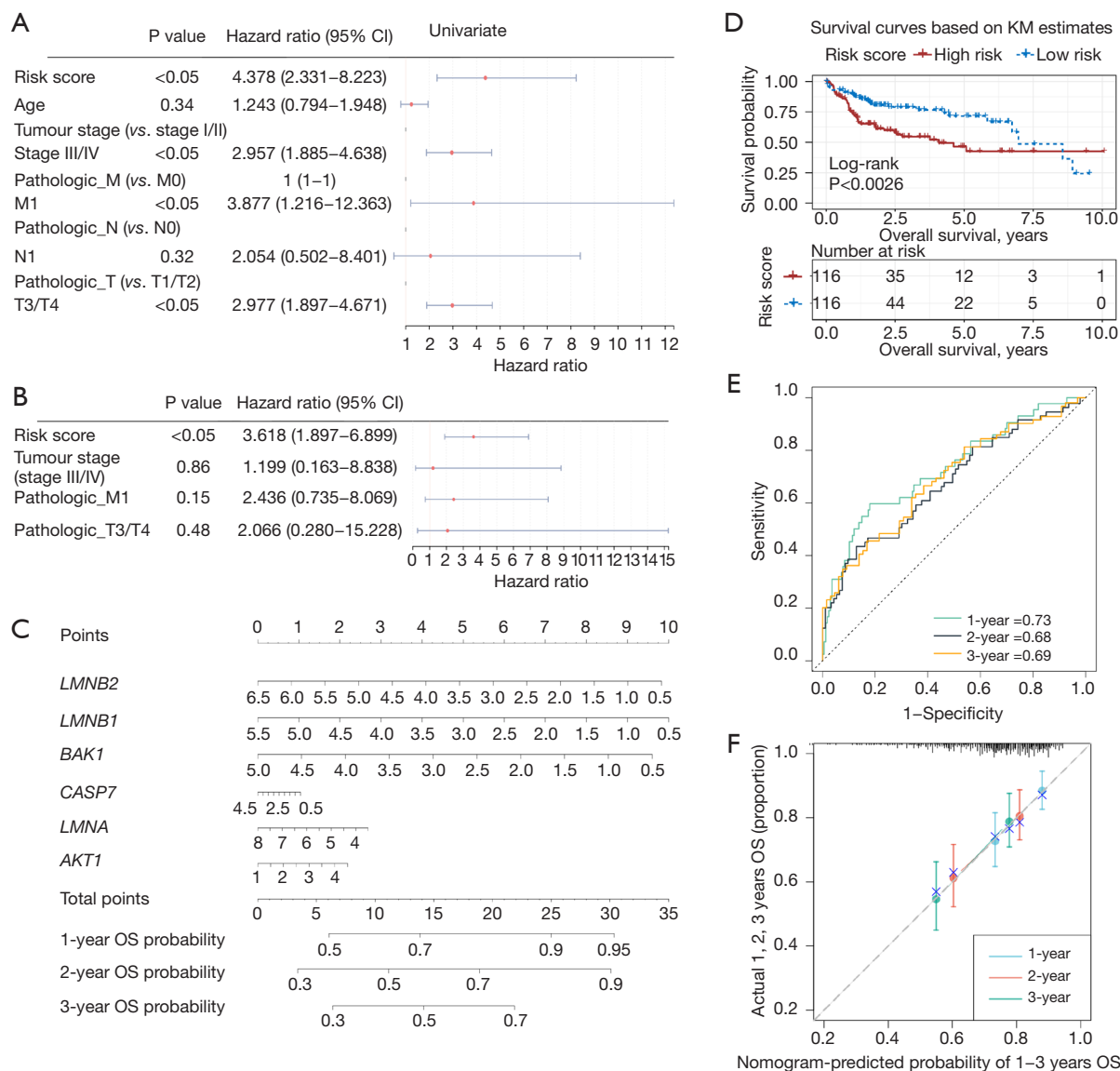


Figure 4 Construction of nomogram. (A) The univariate Cox analysis of the prognostic clinical indicators. (B) The multivariate Cox analysis of the prognostic clinical indicators. (C) The nomogram, (D) KM survival analysis and (E) the ROC curve of the nomogram (1-, 2-, 3-year). (F) The calibration curve of the nomogram (1-, 2-, 3-year). KM, Kaplan-Meier; ROC, receiver operating characteristic; CI, confidence interval; AUC, area under the curve; OS, overall survival.

upregulation in Huh7 and HepG2 cell lines. These results underscored the reliability of our model and suggested an important role for these prognostic genes in the development of HCC. Characteristics of these genes provided valuable biomarkers for diagnosing and treating HCC (Figure 8C–8E).

Discussion

HCC often progresses unnoticed until beyond the optimal treatment window, necessitating enhanced strategies for early screening, diagnosis, and treatment to improve the prognosis of this malignancy. However, current serological markers for diagnosing HCC exhibit limited sensitivity

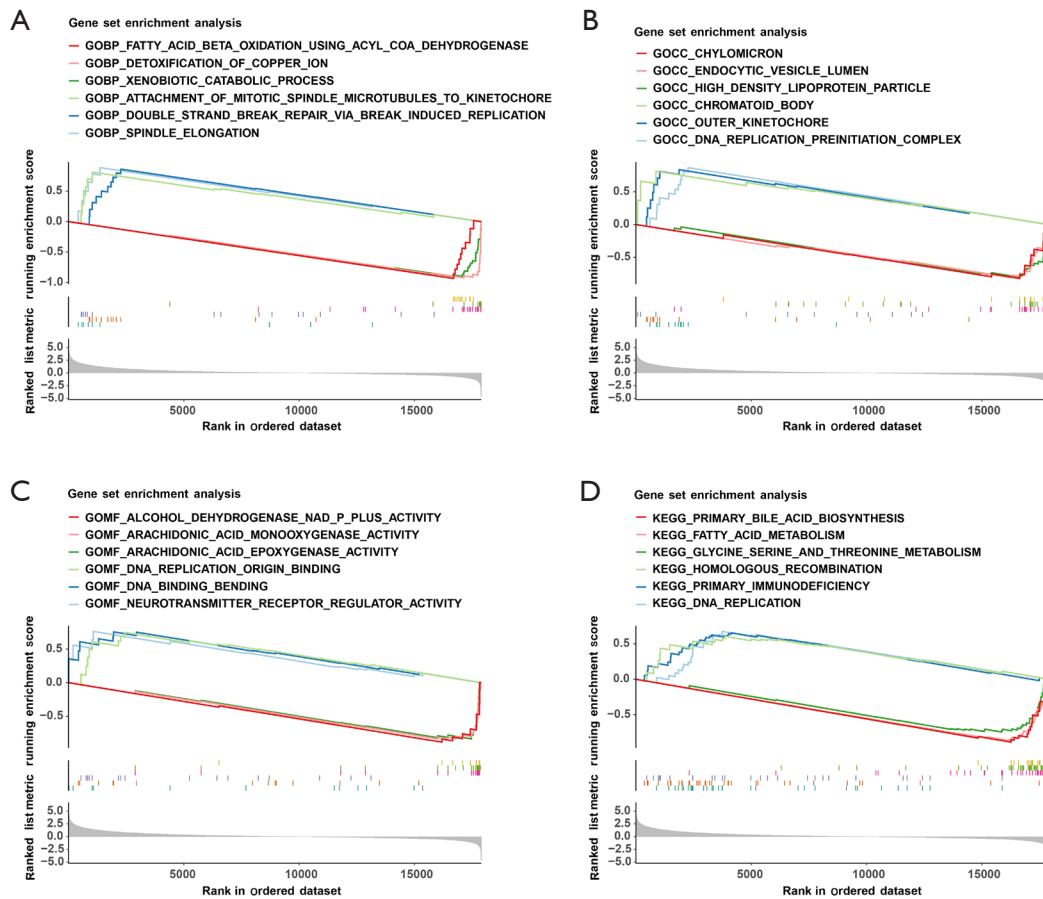


Figure 5 GSEA enrichment analysis between high and low risk groups. (A) Gene-enriched BP pathway; (B) gene-enriched CC pathway; (C) gene-enriched MF pathway; (D) gene-enriched KEGG pathway. GSEA, gene set enrichment analysis; BP, biological process; CC, cellular component; MF, molecular function; KEGG, Kyoto Encyclopedia of Genes and Genomes.

and specificity (22). In this study, prognostic genes were identified through biological analysis methods, serving as the basis for treatment and prognosis in HCC.

Initially, genes differentially expressed in HCC were cross-referenced with 39 MPT-DNRGs, yielding 15 intersecting genes. Subsequent LASSO-Cox regression analysis identified *LMNB2*, *LMNB1*, *BAK1*, *CASP7*, *LMNA*, and *AKT1* as prognostic genes associated with MPT-DNRGs in HCC. Their correlation and accuracy were validated using KM and ROC curves. Furthermore, univariate and multivariate Cox regression analyses identified independent prognostic markers from clinicopathological features and risk scores impacting HCC prognosis.

A nomogram was developed to predict the 1-, 3-, and 5-year survival rates of HCC patients based on these prognostic genes. The nomogram's predictive efficiency was validated through ROC and calibration curves. High

expression of *LMNB2*, *LMNB1*, and *LMNA* was observed in tumor samples across both training and validation sets, consistent with qRT-PCR findings.

BAK1, a pro-apoptotic protein crucial in mitochondrial apoptosis, plays a significant role (23). Knockdown of *BAK1* and *CSE1L* was found to significantly accelerate hepatoma cell death and inhibit proliferation (24).

AKT, a protein kinase, when activated, can promote polyploidy, HCC, and mitotic arrest (25). Additionally, a high-fat diet may enhance *AKT* kinase activity biologically, potentially increasing the risk of nonalcoholic steatohepatitis and liver cancer (2). Caspase, central to the apoptosis mechanism, is part of an evolutionarily conserved family of cysteine-aspartic proteases that coordinate cell regulation and apoptosis (26). It has been reported that polymorphisms in the *Caspase7* gene may affect programmed cell death, leading to genomic instability and variability in cancer

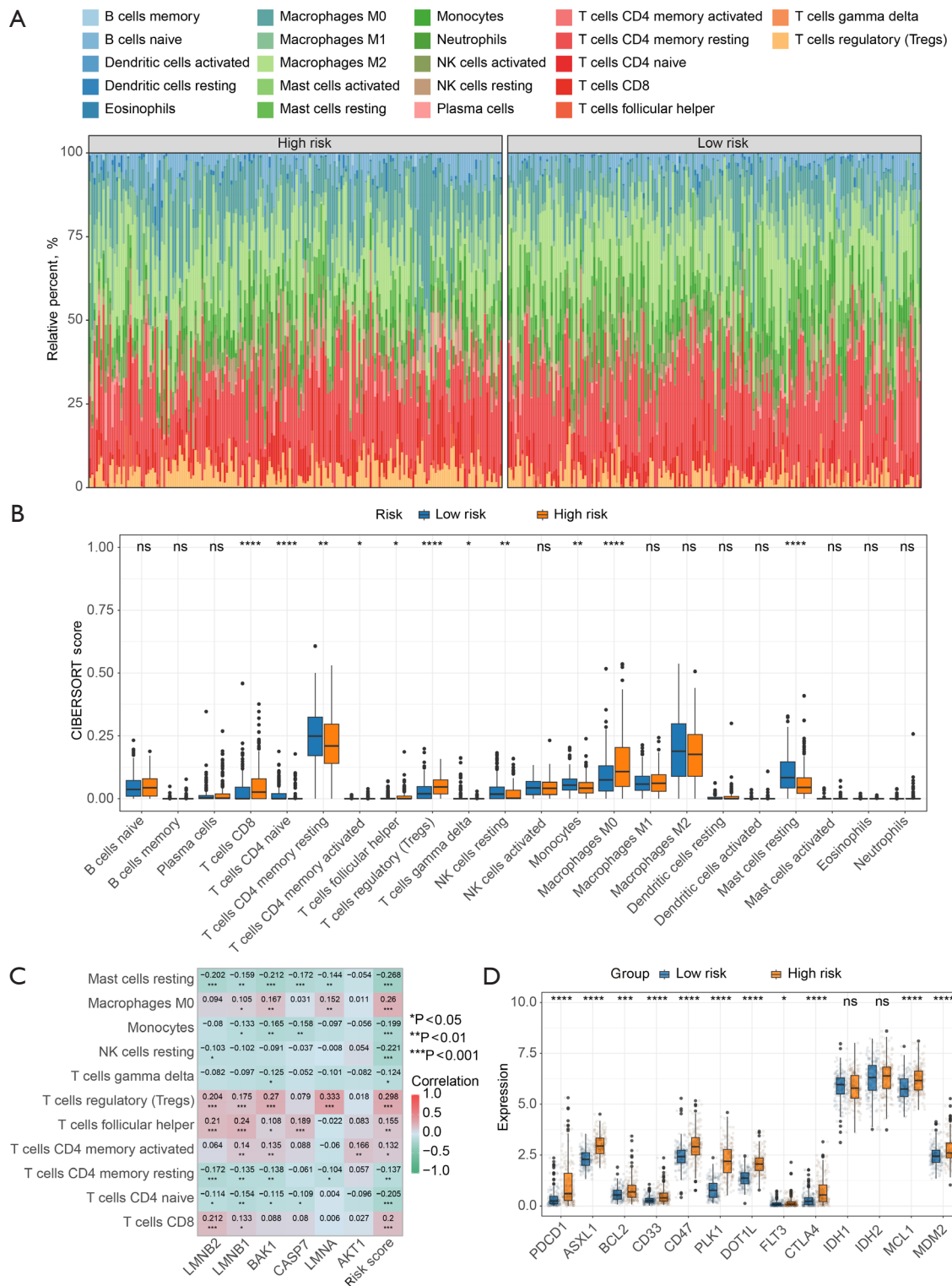


Figure 6 Tumor microenvironment analysis between high-and low-risk groups. (A,B) Heatmap and expression of differential expression of 22 immune cell phenotypes in high-and low-risk groups. (C) Correlation heatmap of prognostic genes with immune cells. (D) The difference of immune checkpoints among risk groups. ns, P>0.05; *, P<0.05; **, P<0.01; ***, P<0.001; ****, P<0.0001.

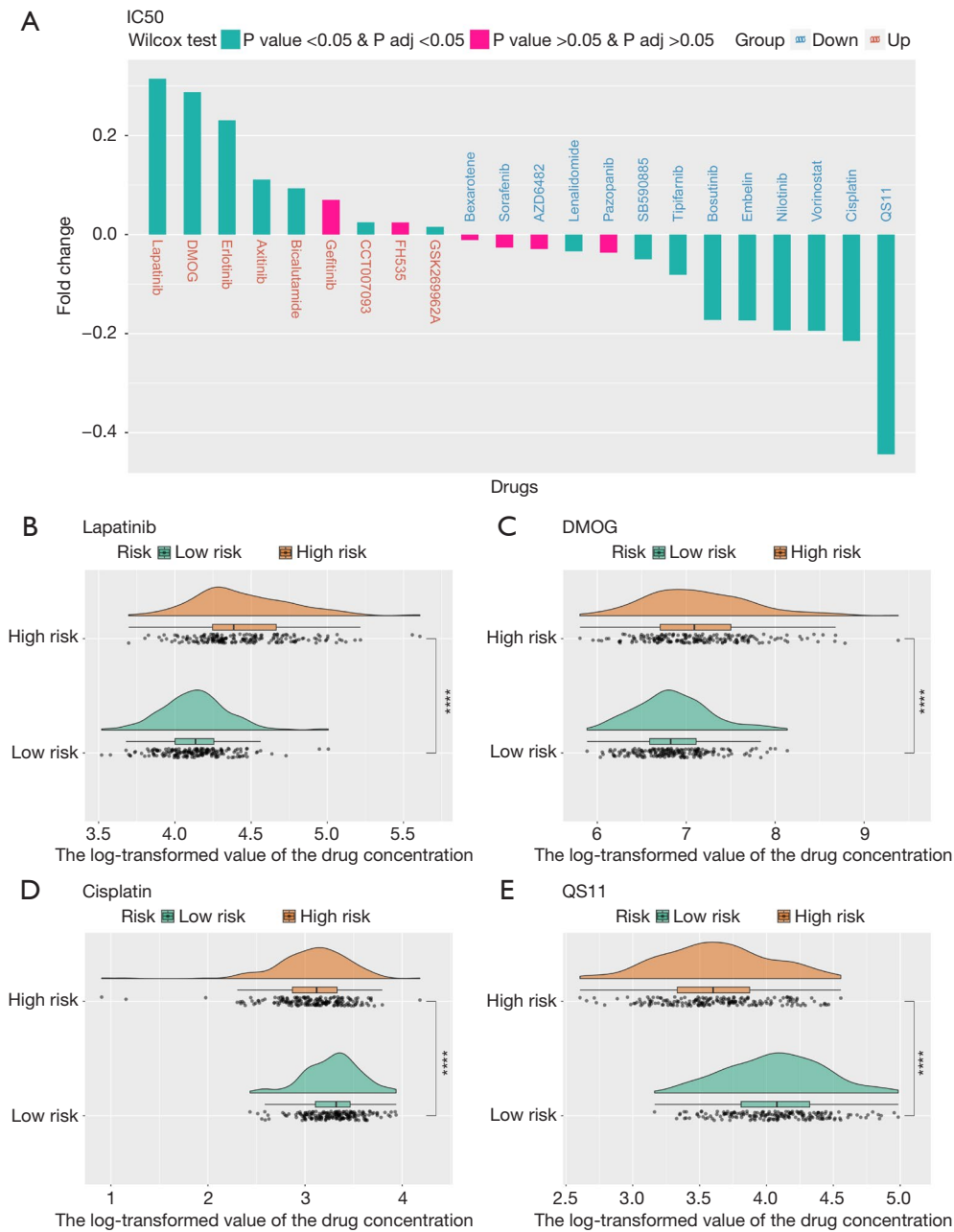


Figure 7 Screen of chemotherapy drugs of HCC. (A) Histogram of differences in drug IC50 values. (B-E) Positive and negative differences between high- and low-risk groups TOP2 drug IC50 values cloud plot. ****, P<0.0001. HCC, hepatocellular carcinoma; IC50, half maximal inhibitory concentration.

susceptibility (27). Laminin primarily constitutes the protein reticulum structure within the inner layer of the nuclear membrane and is involved in various nuclear processes including nuclear migration, apoptosis, cell growth, DNA replication, transcription, and cell cycle regulation (28). Alterations in these genes, essential for

preserving nuclear structure, may result in diseases (29). *LMNB2*, *LMNA*, and *LMNB1* encode the complex network of the nuclear membrane. A study (30) has reported associations between the laminin family and various cancers. Increased *LMNB2* levels are correlated with poor prognosis in HCC. Overexpression of *LMNB1* suggests a

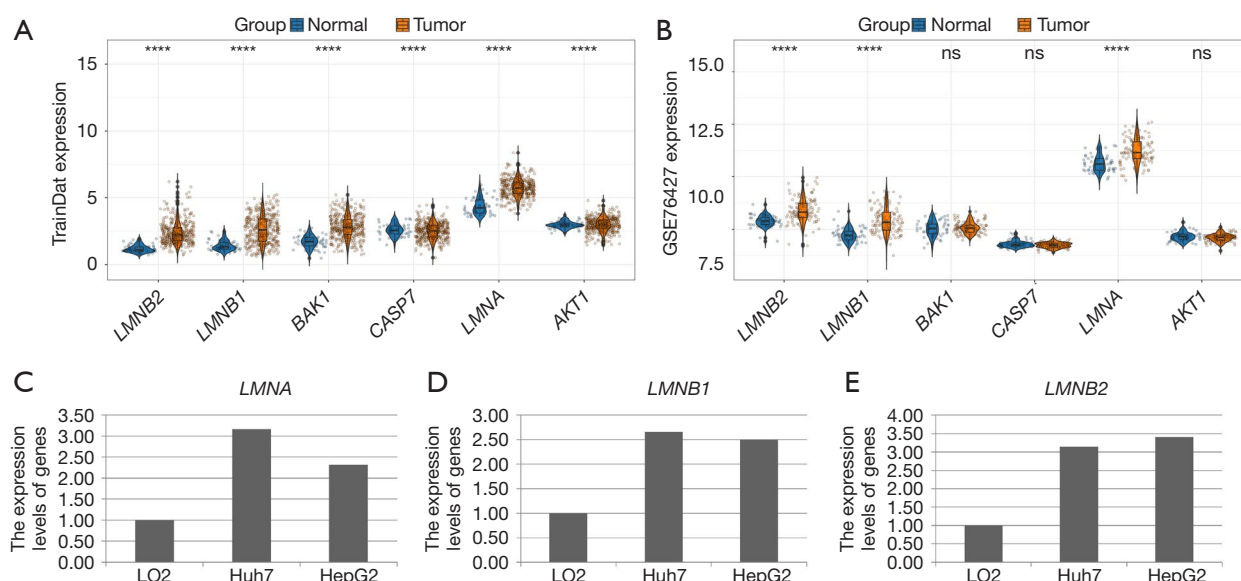


Figure 8 Prognostic gene expression analysis. (A,B) Training set and validation set prognostic genes expression. ns, $P > 0.05$; ****, $P < 0.0001$. (C-E) Prognostic gene expression in the LIHC cell line relative expression level of RT-qPCR results. RT-qPCR, reverse transcription-quantitative polymerase chain reaction; LIHC, liver hepatocellular carcinoma.

poor prognosis in HCC (31), and elevated levels of laminin A are linked with the progression of liver, colorectal, prostate, and ovarian cancers (32-34). Study (35) indicates that the expression of *LMNB2* in primary colorectal cancer tissues and cell lines is significantly higher than in matched non-cancerous tissues and normal colorectal epithelium. Additionally, abnormal expression of the *LMNA* gene in many tumors, particularly in HCC, is associated with decreased survival rates. Knocking out the *LMNA* gene in the HCC cell line HepG2 reduced tumorigenicity, increased P16 expression, and decreased *CDK1* expression (36).

In this study, *LMNB2*, *LMNB1*, and *LMNA* were highly expressed in tumor samples from both the training and validation cohorts. *LMNB2* and *LMNB1*, encoding laminin B2 and B1, respectively, are crucial components of the inner nuclear membrane. They provide essential mechanical support for the nucleus and regulate various cellular functions (37). Previous study (30) has suggested that abnormal expression of *LMNB2* and *LMNB1* may be directly related to uncontrolled cell proliferation and tumorigenesis. In this study, their high expression in HCC further strengthened their possible close relationship with tumor occurrence and development.

Furthermore, GSEA enrichment analysis was employed to explore the potential mechanisms of DEGs. This bioinformatics method revealed significant involvement

in spindle elongation, DNA-binding bending, and DNA replication origin binding. DNA replication is particularly susceptible to damage, leading to replication stress—a hallmark of precancerous and cancerous cells (38). Double-strand breaks (DSBs), the most critical type of DNA damage, must be repaired to maintain genomic integrity and cell viability. Unresolved or improperly repaired DSBs can result in tumorigenesis or cell death. Homologous recombination (HR) and non-homologous end joining are the primary methods for repairing DSBs (39). Primary immunodeficiency, a significant risk factor for HCC (40), often exacerbated by persistent viral infections such as hepatitis B or C, may stem from immunodeficiency (41).

HCC features a critical tumor microenvironment where interactions between immune cells and tumor cells are pivotal for cancer development (42). Our analysis of differences between high- and low-risk groups revealed significant disparities in eleven out of twenty-two immune cell types; regulatory T cells (Treg) exhibited the strongest correlation with the risk score. Furthermore, the correlation between prognostic genes, the risk score, and immune cells was positively higher than with other immune cell types. Key players in the immunological milieu of liver cancer, Treg cells are notably increased in HCC (43). In our examination of immune checkpoints in different risk groups, 11 genes were identified with significantly upregulated

expression, including *PDCD1*, *ASXL1*, *BCL2*, *CD33*, *CD47*, *PLK1*, *DOT1L*, *FLT3*, *CTLA4*, *MCL1*, and *MDM2*. Some studies suggest *CD47* is closely related to HCC (44), and *PLK1* is markedly up-regulated in patients with HCC (45). These findings are consistent with our analysis, suggesting that the overexpression of immune checkpoint molecules and suppression of immune function contribute to the onset of tumor diseases, presenting a new avenue for HCC treatment.

In addition, the nomogram model developed in this study predicts the survival rate of HCC patients and explores the potential clinical application of this model in guiding chemotherapy for HCC. However, drug resistance during chemotherapy remains a primary factor in the suboptimal therapeutic outcomes in HCC, preventing some patients from benefiting from treatment (46). Predicting the clinical efficacy of different chemotherapy agents in advance and selecting highly sensitive drugs could improve the prognosis of HCC patients. Significant differences were observed in the IC50 values of lapatinib, dimethylglycylglycine, cisplatin, and QS11 between the high- and low-risk groups, indicating distinct drug sensitivities which suggest that MPT-DNRGs might play a crucial regulatory role in the responsiveness to certain drugs and influence cancer cell resistance to chemotherapy. It has been reported that a combination of Celastrol and Lapatinib provides a potent synergistic anti-cancer effect in HCC (47), and cisplatin, a standard drug for advanced liver cancer, targets mitochondrial fission factor (MFF) to modulate *Drp1* expression and enhance cisplatin resistance in HCC (48). This model is instrumental in selecting chemotherapy regimens and assessing treatment efficacy, offering valuable guidance for clinical HCC treatment.

However, there are limitations in this study. Although online databases were utilized to validate our model genes with positive outcomes and RT-qPCR analysis was conducted on the final three genes, additional cellular or *in vitro* experiments were not performed to verify expression level differences, thus reducing the credibility of our study. Furthermore, the mechanisms of the model are yet to be explored, necessitating further investigation to aid in the individualized treatment of HCC patients. Future plans include more extensive cellular and *in vitro* studies to thoroughly verify the expression levels of model genes and their role in HCC. These experiments will provide deeper insights into the BPs and enhance our understanding of the model's mechanisms.

Additionally, recognizing the importance of further

exploring the potential therapeutic implications of our findings, we aim to study the role of the model in predicting treatment responses and to develop targeted therapies based on the gene expression profiles of the model. By doing so, we hope to advance personalized treatment strategies for HCC patients, ultimately improving their prognosis and quality of life.

Conclusions

This study explored six prognostic genes (*LMNB2*, *LMNB1*, *BAK1*, *CASP7*, *LMNA* and *AKT1*) associated with MPT-DNRGs in HCC, providing a reference for HCC research.

Acknowledgments

We would like to express our sincere gratitude to all individuals and organizations who supported and assisted us throughout this research. In conclusion, we extend our thanks to everyone who has supported and assisted us along the way. Without your support, this research would not have been possible.

Footnote

Reporting Checklist: The authors have completed the TRIPOD reporting checklist. Available at <https://tcr.amegroups.com/article/view/10.21037/tcr-24-1442/rc>

Peer Review File: Available at <https://tcr.amegroups.com/article/view/10.21037/tcr-24-1442/prf>

Funding: This study was supported by the Excellent Scientific Research Team Project of the First Affiliated Hospital of Jiamusi University (No. 202301) and the Dongji Academic Team of Jiamusi University (No. DJXSTD202410).

Conflicts of Interest: All authors have completed the ICMJE uniform disclosure form (available at <https://tcr.amegroups.com/article/view/10.21037/tcr-24-1442/coif>). The authors have no conflicts of interest to declare.

Ethical Statement: The authors are accountable for all aspects of the work in ensuring that questions related to the accuracy or integrity of any part of the work are appropriately investigated and resolved. The study was conducted in accordance with the Declaration of Helsinki (as

revised in 2013).

Open Access Statement: This is an Open Access article distributed in accordance with the Creative Commons Attribution-NonCommercial-NoDerivs 4.0 International License (CC BY-NC-ND 4.0), which permits the non-commercial replication and distribution of the article with the strict proviso that no changes or edits are made and the original work is properly cited (including links to both the formal publication through the relevant DOI and the license). See: <https://creativecommons.org/licenses/by-nc-nd/4.0/>.

References

- Sung H, Ferlay J, Siegel RL, et al. Global Cancer Statistics 2020: GLOBOCAN Estimates of Incidence and Mortality Worldwide for 36 Cancers in 185 Countries. *CA Cancer J Clin* 2021;71:209-49.
- Bu L, Zhang Z, Chen J, et al. High-fat diet promotes liver tumorigenesis via palmitoylation and activation of AKT. *Gut* 2024;73:1156-68.
- Yang JD, Hainaut P, Gores GJ, et al. A global view of hepatocellular carcinoma: trends, risk, prevention and management. *Nat Rev Gastroenterol Hepatol* 2019;16:589-604.
- Wang X, Lu J. Immunotherapy for hepatocellular carcinoma. *Chin Med J (Engl)* 2024;137:1765-76.
- Raoul JL, Forner A, Bolondi L, et al. Updated use of TACE for hepatocellular carcinoma treatment: How and when to use it based on clinical evidence. *Cancer Treat Rev* 2019;72:28-36.
- Chen L, Sun J, Yang X. Radiofrequency ablation-combined multimodal therapies for hepatocellular carcinoma: Current status. *Cancer Lett* 2016;370:78-84.
- Pinto Marques H, Gomes da Silva S, De Martin E, et al. Emerging biomarkers in HCC patients: Current status. *Int J Surg* 2020;82S:70-6.
- Grandhi MS, Kim AK, Ronnekleiv-Kelly SM, et al. Hepatocellular carcinoma: From diagnosis to treatment. *Surg Oncol* 2016;25:74-85.
- Hou J, Zhang H, Sun B, et al. The immunobiology of hepatocellular carcinoma in humans and mice: Basic concepts and therapeutic implications. *J Hepatol* 2020;72:167-82.
- Ballot C, Kluza J, Lancel S, et al. Inhibition of mitochondrial respiration mediates apoptosis induced by the anti-tumoral alkaloid lamellarin D. *Apoptosis* 2010;15:769-81.
- Galluzzi L, Vitale I, Aaronson SA, et al. Molecular mechanisms of cell death: recommendations of the Nomenclature Committee on Cell Death 2018. *Cell Death Differ* 2018;25:486-541.
- Liu J, Zhang M, Sun Q, et al. Construction of a novel MPT-driven necrosis-related lncRNAs signature for prognosis prediction in laryngeal squamous cell carcinoma. *Environ Sci Pollut Res Int* 2023;30:77210-25.
- Love MI, Huber W, Anders S. Moderated estimation of fold change and dispersion for RNA-seq data with DESeq2. *Genome Biol* 2014;15:550.
- Cao T, Li Q, Huang Y, et al. plotnineSeqSuite: a Python package for visualizing sequence data using ggplot2 style. *BMC Genomics* 2023;24:585.
- Zheng X, Ma Y, Bai Y, et al. Identification and validation of immunotherapy for four novel clusters of colorectal cancer based on the tumor microenvironment. *Front Immunol* 2022;13:984480.
- Yu G, Wang LG, Han Y, et al. clusterProfiler: an R package for comparing biological themes among gene clusters. *OMICS* 2012;16:284-7.
- Liu TT, Li R, Huo C, et al. Identification of CDK2-Related Immune Forecast Model and ceRNA in Lung Adenocarcinoma, a Pan-Cancer Analysis. *Front Cell Dev Biol* 2021;9:682002.
- Yang H, Wang K, Li B, et al. The Prognostic Role of Blood Inflammatory Biomarkers and EGFR Mutation Status in Stage IIIA/N2 Non-Small Cell Lung Cancer Patients Treated With Trimodality Therapy. *Front Oncol* 2021;11:707041.
- Jiang H, Chen H, Wang Y, et al. Novel Molecular Subtyping Scheme Based on In Silico Analysis of Cuproptosis Regulator Gene Patterns Optimizes Survival Prediction and Treatment of Hepatocellular Carcinoma. *J Clin Med* 2023;12:5767.
- Sturm G, Finotello F, List M. Immunedeconv: An R Package for Unified Access to Computational Methods for Estimating Immune Cell Fractions from Bulk RNA-Sequencing Data. *Methods Mol Biol* 2020;2120:223-32.
- Fu D, Zhang B, Wu S, et al. Prognosis and Characterization of Immune Microenvironment in Acute Myeloid Leukemia Through Identification of an Autophagy-Related Signature. *Front Immunol* 2021;12:695865.
- Piñero F, Dirchwolf M, Pessôa MG. Biomarkers in

- Hepatocellular Carcinoma: Diagnosis, Prognosis and Treatment Response Assessment. *Cells* 2020;9:1370.
23. Yang X, Tang S, Li D, et al. DIDS inhibits overexpression BAK1-induced mitochondrial apoptosis through GSK3 β / β -catenin signaling pathway. *J Cell Physiol* 2018;233:5070-7.
 24. Zhu J, Tang B, Lv X, et al. Identifying Apoptosis-Related Transcriptomic Aberrations and Revealing Clinical Relevance as Diagnostic and Prognostic Biomarker in Hepatocellular Carcinoma. *Front Oncol* 2020;10:519180.
 25. Hegde PS, Chen DS. Top 10 Challenges in Cancer Immunotherapy. *Immunity* 2020;52:17-35.
 26. Lamkanfi M, Declercq W, Kalai M, et al. Alice in caspase land. A phylogenetic analysis of caspases from worm to man. *Cell Death Differ* 2002;9:358-61.
 27. Liu CY, Wu MC, Chen F, et al. A Large-scale genetic association study of esophageal adenocarcinoma risk. *Carcinogenesis* 2010;31:1259-63.
 28. Camps J, Erdos MR, Ried T. The role of lamin B1 for the maintenance of nuclear structure and function. *Nucleus* 2015;6:8-14.
 29. Shin JY, Dauer WT, Worman HJ. Lamina-associated polypeptide 1: protein interactions and tissue-selective functions. *Semin Cell Dev Biol* 2014;29:164-8.
 30. Kong W, Wu Z, Yang M, et al. LMNB2 is a prognostic biomarker and correlated with immune infiltrates in hepatocellular carcinoma. *IUBMB Life* 2020;72:2672-85.
 31. Yang Y, Gao L, Chen J, et al. Lamin B1 is a potential therapeutic target and prognostic biomarker for hepatocellular carcinoma. *Bioengineered* 2022;13:9211-31.
 32. Kong L, Schäfer G, Bu H, et al. Lamin A/C protein is overexpressed in tissue-invading prostate cancer and promotes prostate cancer cell growth, migration and invasion through the PI3K/AKT/PTEN pathway. *Carcinogenesis* 2012;33:751-9.
 33. Willis ND, Cox TR, Rahman-Casañs SF, et al. Lamin A/C is a risk biomarker in colorectal cancer. *PLoS One* 2008;3:e2988.
 34. Liu H, Li D, Zhou L, et al. LMNA functions as an oncogene in hepatocellular carcinoma by regulating the proliferation and migration ability. *J Cell Mol Med* 2020;24:12008-19.
 35. Dong CH, Jiang T, Yin H, et al. LMNB2 promotes the progression of colorectal cancer by silencing p21 expression. *Cell Death Dis* 2021;12:331.
 36. Liu H, Li DM, Zhu LY, et al. Research on the knockout of LMNA gene by CRISPR/Cas9 system in human cell lines. *Yi Chuan* 2019;41:66-75.
 37. Yang SH, Chang SY, Yin L, et al. An absence of both lamin B1 and lamin B2 in keratinocytes has no effect on cell proliferation or the development of skin and hair. *Hum Mol Genet* 2011;20:3537-44.
 38. Gaillard H, García-Muse T, Aguilera A. Replication stress and cancer. *Nat Rev Cancer* 2015;15:276-89.
 39. Li J, Sun H, Huang Y, et al. Pathways and assays for DNA double-strand break repair by homologous recombination. *Acta Biochim Biophys Sin (Shanghai)* 2019;51:879-89.
 40. Kebudi R, Kiykim A, Sahin MK. Primary Immunodeficiency and Cancer in Children; A Review of the Literature. *Curr Pediatr Rev* 2019;15:245-50.
 41. Zhang CH, Cheng Y, Zhang S, et al. Changing epidemiology of hepatocellular carcinoma in Asia. *Liver Int* 2022;42:2029-41.
 42. Ho DW, Tsui YM, Chan LK, et al. Single-cell RNA sequencing shows the immunosuppressive landscape and tumor heterogeneity of HBV-associated hepatocellular carcinoma. *Nat Commun* 2021;12:3684.
 43. Zheng C, Zheng L, Yoo JK, et al. Landscape of Infiltrating T Cells in Liver Cancer Revealed by Single-Cell Sequencing. *Cell* 2017;169:1342-1356.e16.
 44. Kim H, Bang S, Jee S, et al. Clinicopathological significance of CD47 expression in hepatocellular carcinoma. *J Clin Pathol* 2021;74:111-5.
 45. Wang YC, Tian ZB, Tang XQ. Bioinformatics screening of biomarkers related to liver cancer. *BMC Bioinformatics* 2021;22:521.
 46. Chen S, Cao Q, Wen W, et al. Targeted therapy for hepatocellular carcinoma: Challenges and opportunities. *Cancer Lett* 2019;460:1-9.
 47. Yan YY, Guo Y, Zhang W, et al. Celastrol enhanced the anticancer effect of lapatinib in human hepatocellular carcinoma cells in vitro. *J BUON* 2014;19:412-8.
 48. Li X, Wu Q, Ma F, et al. Mitochondrial fission factor promotes cisplatin resistance in hepatocellular carcinoma. *Acta Biochim Biophys Sin (Shanghai)* 2022;54:301-10.

Cite this article as: Jin J, Wang M, Liu Y, Li W, Zhang X, Cheng Z. Mitochondrial permeability transition drives the expression, identification and validation of necrosis-related genes in prognostic risk models of hepatocellular carcinoma. *Transl Cancer Res* 2025;14(2):1037-1052. doi: 10.21037/tcr-24-1442